

IR emission spectra of burning shed cedar needles

R.Sh. Tsvyk

*Institute of Atmospheric Optics,
Siberian Branch of the Russian Academy of Sciences, Tomsk*

Received May 4, 2007

The experimental results of studying the flame spectra (1.5–5 μm) of burning shed cedar needles are presented. The flame emission spectrum has significant peaks in absorption (emission) bands of CO_2 and H_2O . Most emission lines remained unassigned, because they belong to various gases generated as a result of burning and pyrolysis.

Introduction

It is well-known¹ that smoggy luminous flame emits analogously to the black body (BB). Soot particles and particles of atmospheric aerosol involved in the flame serve as sources of the continuum emission spectrum. The temperature of particles is close to the temperature of the carrier gas. A main feature of emission of the flame without particles (dark flame) is the selectivity, that is, a capability of emitting the energy only in certain bands of the electromagnetic spectrum.

The commonly accepted model of the emission of forest fires^{1,2} is the emission of a gray body $R_g(\lambda, T)$, W/cm^2 , with the emission coefficient $\varepsilon \approx 0.5$, which depends on a wavelength in the general case

$$R_g(\lambda, T) = \varepsilon(\lambda) R(\lambda, T) = \frac{A_1 \varepsilon(\lambda) \lambda^{-5}}{\left(\exp\left(\frac{A_2}{\lambda T \cdot 10^{-4}}\right) - 1 \right)}, \quad (1)$$

where $R(\lambda, T)$ is the black body emission, whose spectrum is described by the Planck function; λ is the radiation wavelength, μm ; $A_1 = 3.739 \cdot 10^8 \text{ W}/\text{cm}^2$ and $A_2 = 1.4388 \text{ W}/\text{cm}^2$ are constant coefficients; T is the body temperature in K.

The emission spectrum of the flame from burning forest combustible materials is intermediate, that is, peaks of pyrolysis and burning products are observed in emission bands against the background of the continuum emission spectrum of particles.

Aerosol particles, final and intermediate gaseous burning products are produced permanently in the burning process. The composition and spatial distribution of the concentration of these components usually cannot be determined to a sufficient accuracy. The problem becomes even much more complex, if we take into account that the processes continuously fluctuate in time and space. At the same time, radiative and optical characteristics (absorption and emission coefficients) of the flame and smokes depend on the distribution of chemical components, aerosols, and temperature in the zone of flame and flameless (in rear of the flame front) burning. One should also

take into account the variation of absorption (emission) spectra of gases at high temperatures, since under these conditions new lines may appear, while lines traditional for standard temperatures may weaken, change, or disappear. The problem of emission and absorption spectra of high-temperature gases produced as a result of chemical reactions remains open.

The complexity and ambiguity of absorption and emission processes, generation of aerosol particles, and chemical oxidation processes upon burning of forest combustible materials require further experimental investigations of optical and physical characteristics of such media. This information is necessary for estimation of the influence of fires on atmospheric processes⁴ and development of a model of the spectral composition of radiation in different directions, which would allow us to refine the mathematical model of forest fires and to calculate the influence of thermal flux on neighboring combustible materials and the probability of their ignition.³

This paper presents the results of experimental investigations of flame emission spectra in the spectral range 1.5–5 μm .

Instrumentation

The investigations were carried out on a table placed in a chamber of 10 m in diameter and 16 m in length. The chamber was equipped with two vent holes each 600 mm in diameter. The experimental conditions allowed us to model a ground forest fire at natural convection without wind. The $0.8 \times 3.6 \text{ m}$ table was covered by a 200-mm soil layer. A weighted sample of a forest combustible material was laid uniformly on the $0.4 \times 0.5 \text{ m}$ area. The flame front moved to a monochromator, and this provided the maximal intensity of the spectrum at the exit slit of the monochromator as the front passed through the plane of sharp image.

The emission spectra were recorded on a modernized MDR-6U monochromator with replaceable diffraction gratings and single spectrum decomposition. A disk modulating the light flux with

a frequency of 100 Hz and a KBr lens with a passband of 0.25–20 μm , which formed the image of the measurement zone on the slit, were installed in front of the monochromator entrance slit up to 1 mm wide. An FUO–614-5 photodetector sensitive in the range 1–6 μm was set behind the exit slit of the monochromator, in front of which the emission spectrum was scanned. The photodetector signal was sent to a selective amplifier, detected, digitized by a 12-bit ADC, inputted into a computer, and processed. A factory system built in the monochromator provided the scan time of tens minutes. After modernization of the monochromator, the spectral scan time was equal to 6.4 s. The necessity to increase the scan rate was dictated by two requirements. The first one is the short time of the burning process and its spatiotemporal fluctuations. The second one is caused by the fact that due to the motion of the burning front the studied zone falls within the region of sharp image (region of the maximal intensity at the exit from the monochromator) only for 10–20 s. During the calibration, a model of the BB source of radiation (a rod of silit (silicon carbide) – material used for radiation sources in spectrometers) was set in this region. The grating was turned uniformly, ensuring the linear spectral scan with an error no higher than 3%. Wavelength calibration was carried out against the results of measurement with narrowband filters and against absorption lines of atmospheric water vapor (H_2O) and carbon dioxide (CO_2).

To obtain actual emission spectra, it is necessary to know the spectral sensitivity of the photodetector $S_n(\lambda)$, the spectral composition of the BB radiation $S_u(\lambda)$, the transfer coefficient of the monochromator with a particular grating and the used optics $S_m(\lambda)$, and the atmospheric transfer coefficient $S_a(\lambda)$. To take into account the spectral transfer coefficient of the photoreceiving system, including the transfer coefficient of the atmospheric part of the path $f(\lambda) = S_n(\lambda)S_m(\lambda)S_u(\lambda)$, it was assumed that the black body emits according to the Planck law (1). Then

$$f(\lambda) = U_u(\lambda)/U_{\text{calc}}(\lambda), \quad (2)$$

where $U_{\text{exp}}(\lambda)$ and $U_{\text{calc}}(\lambda)$ are the measured and calculated (accurate to a constant factor A_1) spectra.

The calculation of the transfer coefficients for each of the gratings has allowed us to correct the emission spectra, including the influence of absorption by atmospheric gases on almost 1-m long path between the flame and the photodetector of the monochromator.

Figure 1 shows an example of the measured spectral transfer coefficient $f(\lambda)$ at a BB temperature of 1500 K and the spectral transmittance of the atmosphere $T_{\text{tr}}(\lambda)$, which was calculated using the Internet-accessible IAO SB RAS Information System “Spectroscopy of Atmospheric Gases” (<http://spectra.iao.ru>).

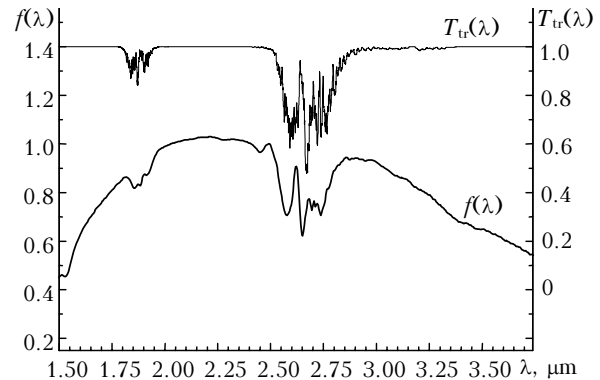


Fig. 1. Transfer coefficient $f(\lambda)$ measured with a 300 lines/mm grating and calculated spectral dependence of transmittance $T_{\text{tr}}(\lambda)$ of the standard atmosphere for summer conditions at a 1-m long path.

All following calculations of the absorption and emission coefficients were performed with the use of this information system and the Internet-accessible Information System “Carbon Dioxide Spectroscopic Databank (CDSD)” for calculation of CO_2 at high temperatures (<http://cdsd.iao.ru/>). The BB temperature was determined by an optical pyrometer with a tungsten filament and a thermocouple. It follows from the data that the total amplitude error of spectral measurements is $\sim \pm 5\%$. Attenuation of the signal in the range 1.81–1.95 and 2.5–2.8 μm is caused by atmospheric H_2O and CO_2 absorption, which is significant even at the total length of the source–detector path of about 1 m.

Experimental results

Figures 2a and b exemplify the flame emission spectra in the range 1.5–3.5 μm (600 lines/mm grating) and 2.65–5.5 μm (300 lines/mm grating) recorded during the burning of shed cedar needles. Figure 2c shows the average emission spectrum of burning domestic gas at a rather stable flame burning. The signal values (in mV) normalized to the transfer coefficient of the corresponding grating are plotted on the ordinate. For comparison, the figures show the calculated (accurate to a constant factor) BB emission spectra with temperature indicated. Some spectra in Figs. 2a, b correspond to different parts of the burning front. As the fire front approaches the monochromator, the level of the signal increases.

Figure 2d shows the calculated spectral transmittance of the standard atmosphere $T_{\text{tr}}(\lambda)$ at $T = 300$ K on a 1-m long path, relative spectral emission coefficients of the standard atmosphere at $T = 1000$ K on the 0.1-m path (thickness of the burning front) taking into account the spectral transmittance of the atmosphere, nitrous oxide N_2O , and methane CH_4 at a room temperature (we failed to find the data for high temperatures). Since the gas concentrations are unknown, constant factors are introduced to make the calculated spectral emission coefficients closer.

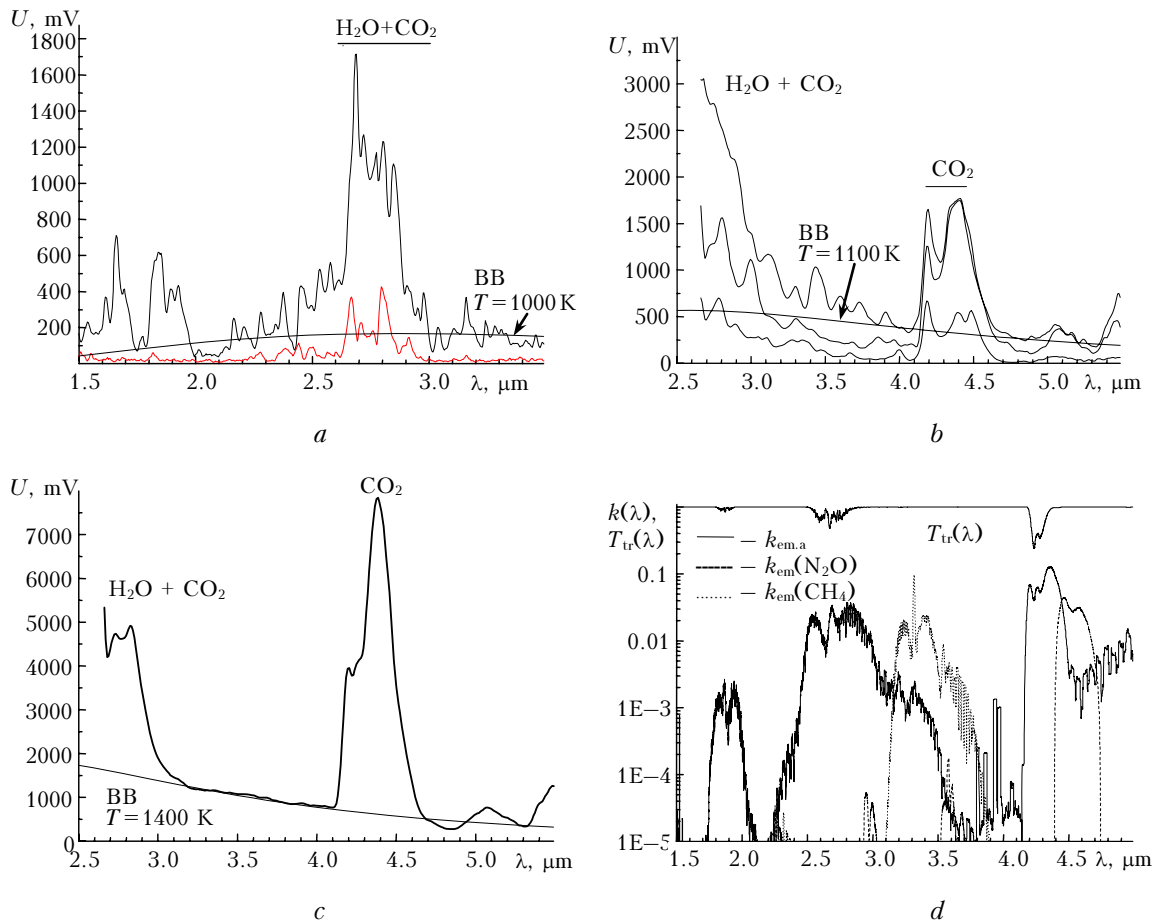


Fig. 2. Emission spectra of flame from burning shed cedar needles (*a*, *b*); from burning domestic gas (*c*); calculated spectral transmittance of the standard atmosphere $T_{tr}(\lambda)$ (*d*), relative emission coefficients of the standard atmosphere $k_{em.a} = k_{em}T_{tr}(\lambda)$ (k_{em} is the emission coefficient neglecting the atmosphere) taking into account the transmission coefficient of the external atmospheric path (beyond the flame); $k_{em}(N_2O)$ and $k_{em}(CH_4)$ are the emission coefficients of N_2O and CH_4 at $T = 300$ K.

From Figs. 2*a,b* and from the comparison with the calculated emission coefficients (Fig. 2*d*), we can see that the flame emission spectrum (against the background of the particulate continuum spectrum) close (in shape) to the BB emission spectrum) includes peaks in emission bands of burning products. In Figs. 2*a,b*, we can clearly see the emission bands of the main burning products: H_2O and CO_2 (for CO_2 , bands centered at 2.7 and 4.3 μm ; for H_2O , bands at 1.87 and 2.7 μm). The signal amplitude at these peaks is roughly 5 to 10 times higher than the BB spectrum. The strong bands at 2.7 and 4.3 μm appear in the first turn.

The flame emission spectrum from burning domestic gas (Fig. 2*c*) includes no significant emission bands except for those of H_2O and CO_2 . The spectra formed from burning shed needles are more complex. The following gases may presumably contribute to this spectrum: nitrous oxide N_2O – strong band at 4.4–4.7 μm and weaker bands at 3.5–3.65, 3.16–3.24, 2.9–3.1, and 2.25–2.3 μm ; NO_2 – band at 3.4–3.5 μm ; hydrocarbons – band centered at 3.3 μm ; CO – emission bands at 4–4.6 μm and

4.6–5.0 μm ; OH radicals having the great number of emission lines from the visible region to 4.5 μm . In Ref. 4, it is reported that the grass combustion products include H_2O , CO_2 , hydrocarbons, nitric oxide, methanol, acetic and formic acids, formaldehyde, and hydroxycetaldehyde. The sources of burning gases are hemicellulose containing six-carbon $C_6H_{10}O_5$ and five-carbon $C_5H_8O_4$ links, as well as cellulose, i.e., polysaccharide of the $(C_6H_{10}O_5)_n$ type. Upon heating, they decompose into CO , H_2O , and CH_4 . The composition of forest materials include also lignin, which is a stable high-molecular compound filling the intercellular space and whose structure is not fully known, and chlorophyll in tree waste and in gum of conifers.³

The absorption band of atmospheric CO_2 (center at 4.3 μm), which is compensated upon consideration of the transfer coefficient, is clearly seen in the spectra. However, rather strong absorption is observed in the emission spectrum in this region (Figs. 2*b* and 3*a*). It may be caused by the volume distribution of the concentration of absorbing gases, mostly CO_2 , generated in the burning process. The

absorption and emission coefficients depend on temperature, whose distribution along the direction of motion of the fire front is close to Gaussian.^{6,7}

In Ref. 5, the capability of observing the flame emission spectrum through the atmosphere in the range 4–5 μm is presented as an example. In that case, the circumstance is used that the width of the flame emission band is much wider than the atmospheric absorption band. Figure 3 shows the results of analogous analysis through the comparison of the calculated transmittance of the standard atmosphere at $T = 296$ K on a 1000-m path with the calculated spectral emission coefficient of a 0.1-m thick gas layer at $T = 1000$ K and the experimental flame emission spectrum from burning shed cedar needles and burning domestic gas taking into account the transmittance at the 1-m long measurement path. The calculated and the experimental spectra are normalized to the maximum value.

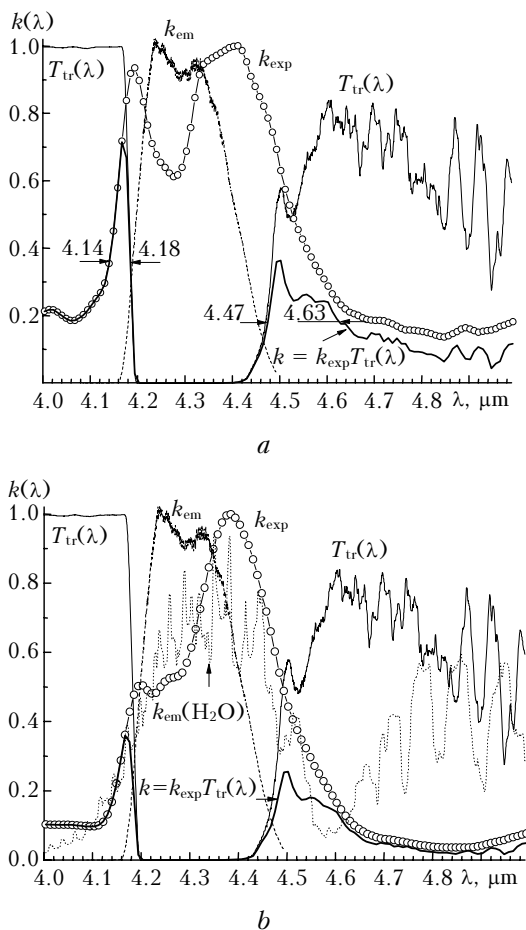


Fig. 3. Atmospheric transmission spectrum $T_{tr}(\lambda)$ in the absorption band at 4–5 μm for the summer atmosphere on a 1000-m path. Calculated emission coefficient of a gas layer k_{em} for CO_2 and $k_{em}(\text{H}_2\text{O})$ for H_2O at $T = 1000$ K; experimental flame emission spectrum from burning shed cedar needles k_{exp} (a) and domestic gas (b); expected experimental flame emission spectrum at a distance of 1000 m $k = k_{exp}T_{tr}(\lambda)$. All the emission spectra are normalized to the maximal values.

It should be noted that in our measurements the experimental flame emission spectrum is much wider than the calculated one and close to the spectrum presented in Ref. 5. The emission spectra after the propagation through the atmosphere coincide as well. The obtained results show that the ranges 4.14–4.18 μm and 4.48–4.63 μm are promising for detection of the tree waste flame. The range 4.14–4.18 μm can be extended to 3.5–4.18 μm taking into account the atmospheric transmission band and the rather intense continuum flame emission spectrum. The analogous results have been obtained from the analysis of the flame emission spectrum from burning domestic gas. In this case, the experimental spectrum is narrower than the spectrum of burning shed needles.

The emission spectrum of shed needles (Fig. 3a) at a half-maximum level is wider than the calculated one by 0.045 μm in the range 4.2 μm and by 0.2 μm in the range 4.5 μm . This is likely caused by the contribution of other gases, for example, H_2O vapor [emission band at wavelength higher than 4 μm (Fig. 3b)], N_2O , and CO , having emission bands in this region, to the total emission. The broadening of the experimental spectrum may be connected with the fact that the high temperature of CO_2 is caused not only by its heating, but also by its formation as a result of chemical reaction upon burning of hydrocarbons and carbon monoxide CO .

For the range 1.5–3.5 μm , figure 4 shows the results of analysis similar to that in Fig. 3.

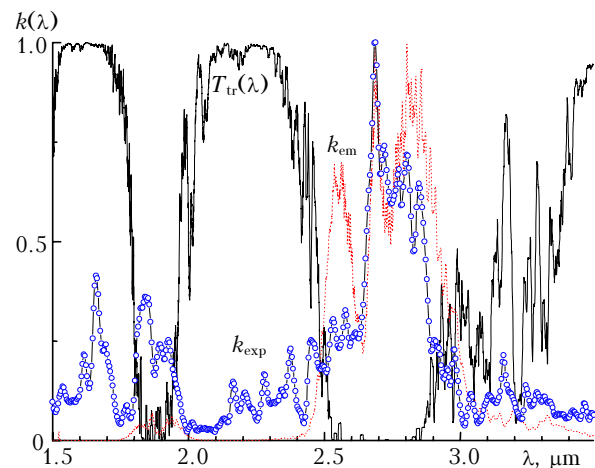


Fig. 4. Atmospheric transmission spectrum $T_{tr}(\lambda)$ in the absorption band 1.5–3.5 μm for the summer atmosphere on a 1000-m path. Calculated emission coefficient k_{em} of the atmosphere at $T = 1000$ K, and experimental flame emission spectrum k_{exp} from burning shed needles, both normalized to the maximal values.

One can see that the experimental spectrum is narrower than the calculated one in the band 2.5–3 μm . In contrast to the 4–5 μm band, the experimental emission spectrum does not go beyond the absorption band, and therefore the recording of flame is worth being conducted in the well-known

and widely used atmospheric transmission bands: 1.5–1.8, 2–2.5, and 3.5–4 μm .

Conclusions

1. The complex structure of the flame emission spectrum from burning forest materials is caused by thermochemical processes, as a result of which the burning products (CO_2 , H_2O) are the main emission sources. Additional lines in the flame emission spectrum may originate from various nitrogen and hydrocarbon compounds, radicals, etc.

2. In the IR region, the emission bands of carbon dioxide CO_2 (nearby 4.3 and 2.7 μm) and water vapor H_2O (nearby 1.9 and 2.7 μm) were identified successfully in the flame spectrum. In the range 4–5 μm , the width of the emission band exceeds that of the calculated emission spectrum at $T = 1000$ K and the width of the atmospheric absorption band. In the experimental BB emission spectra, one can clearly see the absorption band of atmospheric CO_2 at a wavelength of 4.3 μm (analogously to the data of Fig. 1), which is compensated when taking into account the transfer coefficient on the atmospheric part of the path.

However, rather strong absorption remains in the emission spectrum in this range (a dip at the CO_2 absorption wavelength at 4.3 μm in Fig. 2b), and this absorption is likely caused by the absorption by CO_2 generated in the flame as a result of the burning process.

References

1. L.Z. Kriksunov, *Reference Book on Principles of Infrared Technology* (Sov. Radio, Moscow, 1978), 400 pp.
2. L.A. Mirzoeva, G.B. Kameshkov, E.L. Lustberg, G.A. Makovtsev, and G.V. Zakharenkov, *Opt. Zh.*, No. 8, 17–21 (1992).
3. A.M. Grishin, *Mathematical Simulation of Forest Fires and New Fire Fighting Methods* (Nauka, Novosibirsk, 1992), 406 pp.
4. K.Ya. Kondratyev and V.A. Isidorov, *Atmos. Oceanic Opt.* **14**, No. 2, 93–101 (2001).
5. G. Gaussorgues, *La Thermographie Infrarouge: Principes, Technologies, Applications* (TEC DOC, 1999), 608 pp.
6. A.M. Grishin and R.Sh. Tsvyk, in: *Proc. of the Fifth Minsk Int. Forum of Heat and Mass Exchange* (Minsk, 2004), Vol. 1, pp. 170–172.
7. A.M. Grishin and R.Sh. Tsvyk, *J. Heat Transfer Res.* **36**, No. 7, 529–542 (2005).